Quasi-Ray Gaussian Beam Algorithm for Time-Harmonic Two-Dimensional Scattering by Moderately Rough Interfaces

Vincenzo Galdi, *Member, IEEE*, Leopold B. Felsen, *Life Fellow, IEEE*, and David A. Castañon, *Senior Member, IEEE*

***Abstract*—Gabor-based Gaussian beam (GB) algorithms, in conjunction with the complex source point (CSP) method for generating beam-like wave objects, have found application in a variety of high-frequency wave propagation and diffraction scenarios. Of special interest for efficient numerical implementation is the noncollimated narrow-waisted species of GB, which reduces the computationally intensive complex ray tracing for collimated GB propagation and scattering to quasi-real ray tracing, without the failure of strictly real ray field algorithms in caustic and other transition regions. The Gabor-based narrow-waisted CSP-GB method has been applied previously [1]–[3] to two-dimensional (2-D) propagation from extended nonfocused and focused aperture distributions through arbitrarily curved 2-D layered environments. In this 2-D study, the method is applied to aperture-excited field scattering from, and transmission through, a moderately rough interface between two dielectric media. It is shown that the algorithm produces accurate and computationally efficient solutions for this complex propagation environment, over a range of calibrated combinations of the problem parameters. One of the potential uses of the algorithm is as an efficient forward solver for inverse problems concerned with profile and object reconstruction [4].**

***Index Terms*—Gabor lattice representations, Gaussian beams, rough surface scattering.**

I. Introduction

REFLECTION from, and transmission through, a rough (irregular) boundary separating two different material media is of interest in many applications. One such application is the detection and classification of buried objects using ground-penetrating radar. This application involves above-ground transmitters and receivers. The twice-traversed air–ground interface is a principal corruptor of the signal on its way to and from the targets of interest. To enhance the detection and classification processing, it is important to model the distortion introduced by the air–ground interface.

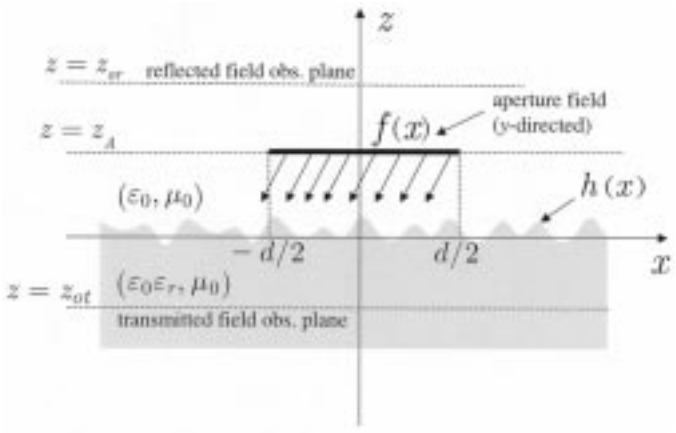

Fig. 1. Problem geometry. An incident field from an extended tapered aperture field distribution at $z = z_A$ is assumed to impinge on a moderately rough interface, described by the continuous function $h(x)$, separating free space and a dielectric half-space. Reflected and transmitted fields are observed at $z = z_{or}$ and $z = z_{ot}$, respectively.

As a first step toward this goal, we investigate in this paper the reflection from, and transmission through, a moderately rough (coarse-scale) interface between air and a homogeneous dielectric (soil) half-space (see Fig. 1); this forward problem constitutes an electromagnetic (EM) scattering problem, and inclusion of the transmitted field anticipates the subsequent interest in computing the scattering from buried objects. In a following paper [4], we shall be concerned with the reconstruction (inverse problem) of the interface profile under the realistic constraints of spatially sampled data. A key ingredient in the reconstruction problem is a fast forward model that can relate descriptions of potential interface profiles to the measured signals at the different receiver locations.

The analytic and numerical modeling of wave scattering from rough surfaces constitutes a problem of longstanding interest (see [5]–[13] for a sparse sampling). Our objective in this paper is to develop a fast forward solver, using discretized Gabor-based, high-frequency asymptotic, narrow-waisted Gaussian beam (GB) basis fields in conjunction with the complex source point (CSP) method for generating ray-like GB wave objects [1]–[3]. The Gabor-based narrow-waisted CSP-GB method has been applied previously [1]–[3] to two-dimensional (2-D) field propagation from extended nonfocused and focused one-dimensional (1-D) planar aperture distributions through layered

Manuscript received September 6, 2000; revised February 12, 2001. This work was supported by ODDR&E under MURI Grants ARO DAAG55-97-1-0013 and AFOSR F49620-96-1-0028, and by the Engineering Research Centers Program of the National Science Foundation under Award EEC-9986821. The work of V. Galdi was also supported by a European Union postdoctoral fellowship through the University of Sannio, Benevento, Italy. The work of L. B. Felsen was supported in part by the US-Israel Binational Science Foundation, Jerusalem, Israel, under Grant 9900448 and by Polytechnic University, Brooklyn, NY, USA.

V. Galdi is with the Department of Electrical and Computer Engineering, Boston University, Boston, MA 02215 USA and the University of Sannio, Benevento, Italy (e-mail: vgaldi@bu.edu).

L. B. Felsen is with the Department of Aerospace and Mechanical Engineering and the Department of Electrical and Computer Engineering, Boston University, Boston, MA 02215 USA and the Polytechnic University, Brooklyn, NY 11201 USA (e-mail: lfelsen@bu.edu).

D. A. Castañon is with the Department of Electrical and Computer Engineering, Boston University, Boston, MA 02215 USA (e-mail: dac@bu.edu).

Publisher Item Identifier S 0018-926X(01)06371-2.

planar and cylindrical environments, and has been found to produce accurate, robust, and computationally efficient solutions over a broad range of problem parameters, provided that these do not violate the constraints imposed by the high-frequency asymptotic assumptions. Briefly, the robustness and reliability criteria are *pragmatic*, being based on the insensitivity of the result to "scramblings" (i.e., to different combinations) of the beam and lattice parameters within the constraint domain. Here, we extend this method to 1-D-aperture-excited 2-D field scattering from, and transmission through, a 1-D moderately rough arbitrary interface between two dielectric media. The resulting algorithm for radiated and scattered field synthesis by GB recombination is found to perform as in [1]–[3], but now subject to new restrictions that are stated, as necessary, in the appropriate sections of this paper.

The rest of this paper is organized as follows. In Section II, we summarize the rigorous, self-consistent Gabor-based Gaussian beam algorithm for a general aperture field distribution and the ensemble of paraxially approximated narrow-waisted CSP beams that this excitation generates [1]. Section III deals with the preliminary (canonical) problem of beam reflection from, and transmission through, a curved interface between two homogeneous dielectrics [14]. These constituents have been used previously for beam tracking through planar and curved layered dielectric configurations [2], [3]. In Section IV, we extend the algorithm to the new and more challenging problem of reflection and transmission of the plane-aperture-excited field in the presence of a moderately rough interface separating two homogeneous semi-infinite dielectric media. Extensive numerical simulations calibrate the algorithm within clearly stated constraints and highlight the role of certain critical parameters. Conclusions follow in Section V.

II. Incident Field From an Extended Aperture

A. Problem Statement

Consider a two-dimensional problem where a y-directed electric field with implicit time-harmonic dependence $\exp(-i\omega t)$ and spatial distribution $f(x)$ is assumed to occupy the aperture region $|x| \le d/2$ at $z = z_A$ in free space, as depicted in Fig. 1

$$\mathbf{E}^{\text{inc}}(x, z_A) = f(x)\mathbf{u}_y, \qquad |x| \le d/2,\ z = z_A. \tag{1}$$

Boldface quantities denote vectors and $\mathbf{u}$ denotes a unit vector. The resulting (TM polarized) EM field radiated into the half-space $z < z_A$ can be expressed as a superposition of line-source generated fields (Kirchhoff integration) [15]

$$\mathbf{E}^{\text{inc}}(x, z) = \frac{i}{2}\int_{-d/2}^{d/2} f(x')\frac{\partial}{\partial z}\mathrm{H}_0^{(1)}(k_0 R)\,dx'\mathbf{u}_y \tag{2}$$

$$\mathbf{H}^{\text{inc}} = \frac{1}{i\omega\mu_0}\nabla \times \mathbf{E}^{\text{inc}} = H_x^{\text{inc}}\mathbf{u}_x + H_z^{\text{inc}}\mathbf{u}_z \tag{3}$$

where $k_0 = \omega\sqrt{\epsilon_0\mu_0} = 2\pi/\lambda_0$ is the free-space wavenumber, λ_0 is the free-space wavelength, $\mathrm{H}_0^{(1)}(\cdot)$ is the zeroth-order Hankel function of the first kind (line source Green's function), and

$$R = \sqrt{(x - x')^2 + (z - z_A)^2}. \tag{4}$$

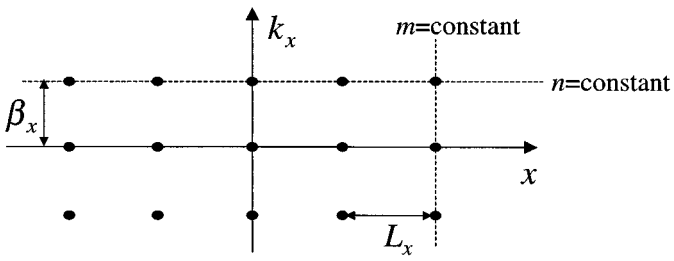

Fig. 2. Discretized phase space lattice. Spatial shift indexes m identify GB launch points at $x = mL_x$. Spectral shift indexes n identify linearly phased GB tilts at $k_x = n\beta_x$.

Because of the polarization assumed in (1), all fields can be generated from the scalar $E = E_y$ component, so that the vector notation will be dropped from here on. Alternatively, by spectral plane wave superposition, one obtains [15]

$$E^{\text{inc}}(x, z) = \frac{1}{2\pi}\int_{-\infty}^{\infty} \hat{f}(k_x)\exp[i(k_x x + k_z z)]\,dk_x \tag{5}$$

where

$$\hat{f}(k_x) = \int_{-\infty}^{\infty} f(x)\exp(-ik_x x)\,dx \tag{6}$$

is the Fourier spectrum of $f(x)$, k_x is the x-domain wavenumber, and

$$k_z = \sqrt{k_0^2 - k_x^2}, \qquad \mathrm{Im}(k_z) \ge 0 \tag{7}$$

is the longitudinal (z-domain) wavenumber.

B. Gabor Beam Discretization

1) Aperture Field: The aperture field $f(x)$ is to be parameterized in terms of Gaussian basis functions via the rigorous self-consistent Gabor series representation [1], [15]–[19]

$$f(x) = \sum_{m,n=-\infty}^{\infty} A_{mn} w(x - mL_x)\exp(in\beta_x x) \tag{8}$$

where $w(x)$ represents the normalized Gaussian window function

$$w(x) = \left(\frac{\sqrt{2}}{L_x}\right)^{1/2}\exp[-\pi(x/L_x)^2], \qquad \int_{-\infty}^{\infty} w^2(x)\,dx = 1. \tag{9}$$

This representation places the aperture distribution on a discretized (x, k_x) phase space lattice (see Fig. 2), with spatial and spectral shifts tagged by the indexes m and n, respectively. Spatial and spectral periods are related by the self-consistency relation (configuration-spectrum tradeoff) [16], [17]

$$L_x\beta_x = 2\pi. \tag{10}$$

As observed in [15] and [19], the Gaussian window provides the best occupation of the phase space. The expansion coefficients A_{mn} in (8) can be computed by introducing an auxiliary function $\gamma(x)$ defined through the *biorthogonality* condition [16], [17]

$$\int_{-\infty}^{\infty} w(x)\gamma^*(x - mL_x)\exp(-in\beta_x x)\,dx = \delta_m\delta_n \tag{11}$$

where * denotes the complex conjugate and $\delta_q = 1$ for $q = 0$ and $\delta_q = 0$ for $q \neq 0$. The expansion coefficients can be written as [16], [17]

$$A_{mn} = \int_{-\infty}^{\infty} f(x)\gamma^*(x - mL_x)\exp(-in\beta_x x)\,dx. \quad (12)$$

For Gaussian windows, the biorthogonal function can be computed explicitly [16], [17] but will not be required in what follows later on.

2) Radiated Field: The initial distribution surrounding each lattice point in Fig. 2 generates a Gaussian beam that is launched from m-indexed locations and tilted according to n-indexed locations. The radiated incident field in the half-space $z < z_A$ [see (2)] therefore admits via (8) a similar discretized representation (we follow the notation in [1]; however, there are some sign changes with respect to [1] since here we assume propagation into the *negative* half-space $z < z_A$)

$$E^{\text{inc}}(x, z) = \sum_{m,n=-\infty}^{\infty} A_{mn}B_{mn}(x, z) \quad (13)$$

where the beam functions $B_{mn}(x, z)$ are expressed by Gabor-weighted line-source superposition

$$B_{mn}(x, z) = \frac{i}{2}\int_{-d/2}^{d/2} w(x' - mL_x) \cdot \exp(in\beta_x x')\frac{\partial}{\partial z}\mathrm{H}_0^{(1)}(k_0 R)\,dx' \quad (14)$$

with R being defined in (4). By saddle point methods, the integral in (14) (or its spectral counterpart) can be evaluated asymptotically in the beam *paraxial far zone*, yielding the following *complex source point* approximation [2], [3]:

$$B_{mn}(x, z) \sim ik_0 2^{5/4}\left(\frac{L_x}{8\pi k_0 \tilde{R}_{mn}}\right)^{1/2} \cdot \exp\left\{i\left[k_0\left(\tilde{R}_{mn} + ib\right) + \pi/4\right]\right\}\frac{(z - \tilde{z}'_{mn})}{\tilde{R}_{mn}} \quad (15)$$

with $\tilde{R}_{mn}$ representing the *complex distance* between the observer at $P = (x, z)$ and the CSP

$$\tilde{P}'_{mn} = (\tilde{x}'_{mn}, \tilde{z}'_{mn}) = (mL_x + ib\sin\theta_n,\ z_A - ib\cos\theta_n) \quad (16)$$

$$\tilde{R}_{mn} = \overline{P\tilde{P}'_{mn}} = \sqrt{(x - \tilde{x}'_{mn})^2 + (z - \tilde{z}'_{mn})^2}. \quad (17)$$

In accord with the radiation condition, the square root in (17) is defined by $\mathrm{Re}(\tilde{R}_{mn}) \geq 0$. Here and henceforth, the tilde $\tilde{}$ identifies CSP-generated complex quantities. The displacement parameter b (equal to the Fresnel length) is related to the beam lattice period L_x and the beam axis angle θ_n via [2]

$$b = (L_x\cos\theta_n)^2/\lambda_0, \qquad \theta_n = \sin^{-1}(n\lambda_0/L_x). \quad (18)$$

Equation (15) is valid in the paraxial far-zone of each beam, $|\tilde{R}_{mn}| \gg b$. As the tilt index n increases, the beam tilt angle θ_n can become complex ($|n| > L_x/\lambda_0$), whence the corresponding beams become *evanescent*.

C. Narrow-Waisted Beams

In the following, we shall focus on nontilted ($n = 0$) *narrow-waisted* beams ($L_x \lesssim \lambda_0 \ll d$), which, as demonstrated in [1]–[3], have several attractive features. First, the Gabor coefficients A_{mn} in (13) can be effectively estimated by *sampling* the aperture field distribution at the lattice points $x = mL_x$, thus avoiding the time-consuming integration in (12) [1]

$$A_{mn} \approx \begin{cases} \left(L_x/\sqrt{2}\right)^{1/2} f(mL_x), & n = 0 \\ 0, & n \neq 0. \end{cases} \quad (19)$$

Under this approximation, the tilted ($n \neq 0$) beams in the Gabor expansion, which here generate evanescent "far fields" [complex θ_n in (18)], are ignored. Second, for narrow-waisted beams, the CSP paraxial far-zone approximation (15) can be invoked at moderate distance; thus their *superposition* can furnish accurate results even in the *near zone* of the *aperture*. Third, as has been shown in [2] and [3], interaction of narrow-waisted beams with an environment can be implemented effectively by tracking the *complex ray* fields and recombining them at the observer, subject to constraints that are elucidated in the examples below.

D. Illustrative Examples

A thorough analysis of the accuracy and computational features of the *narrow-waisted* beam algorithm can be found in [1]. Here, we merely summarize relevant results. Referring to Fig. 1, we consider a linearly phased cosine-tapered aperture field distribution

$$f(x) = \begin{cases} \cos(\pi x/d)\exp(ik_0\nu x), & |x| \leq d/2 \\ 0, & |x| > d/2 \end{cases} \quad (20)$$

where d is the aperture width and $\nu = \sin^{-1}(\varphi)$, with φ denoting the tilt angle of the main radiation lobe with respect to the z-axis. A special case (nonphased cosine, $\nu = 0$) is used in the rough interface simulation in Section IV-B. Fig. 3 shows the normalized magnitude of the exact Gabor coefficients [computed through numerical integration of (12)] as a function of the shift and tilt indexes (m, n) for narrow-waisted beams ($L_x = 0.0125d$). As one can see, the essential contribution comes from the nontilted beams, whose coefficient distribution closely matches the aperture field profile.

The beam-computed and reference near-zone *radiated* fields, which are obtained from (13) [with (15) and (19)], and via numerical evaluation of the Kirchhoff integral in (2), respectively, are shown in Fig. 4(a) for $\nu = 0.5$. Although based on the paraxial far-zone approximation in (15) for the beam propagators, the accuracy is quite good even in the near zone of the aperture (80 beams were used in this simulation). In the absence of phasing ($\nu = 0$), considerably coarser sampling is adequate. As shown in Fig. 4(b), even a beam lattice period $L_x = 0.1d$ (i.e., ten beams) yields accurate synthesis. Coarse sampling also works for linearly phased apertures if propagation-matched *tilted* basis beams are used [20]. The stated number of beams in these simulations was arrived at via the pragmatic "scramblings" test, i.e., when the result remains insensitive to variations in the beam/lattice combinations.

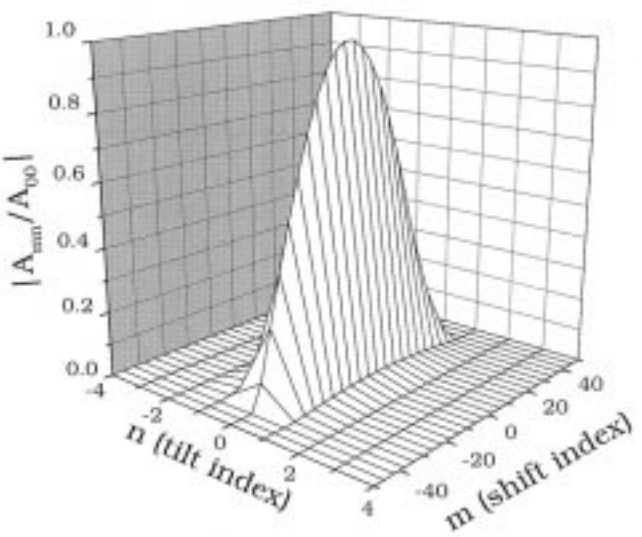

Fig. 3. Linearly phased cosine-tapered aperture field in (20) ($d = 10\lambda_0$, $\nu = 0.5$). Exact normalized Gabor coefficient magnitudes $|A_{mn}/A_{00}|$ in (12) evaluated numerically ($L_x = 0.0125d = 0.125\lambda_0$). Tilted ($n \neq 0$) beams are evanescent.

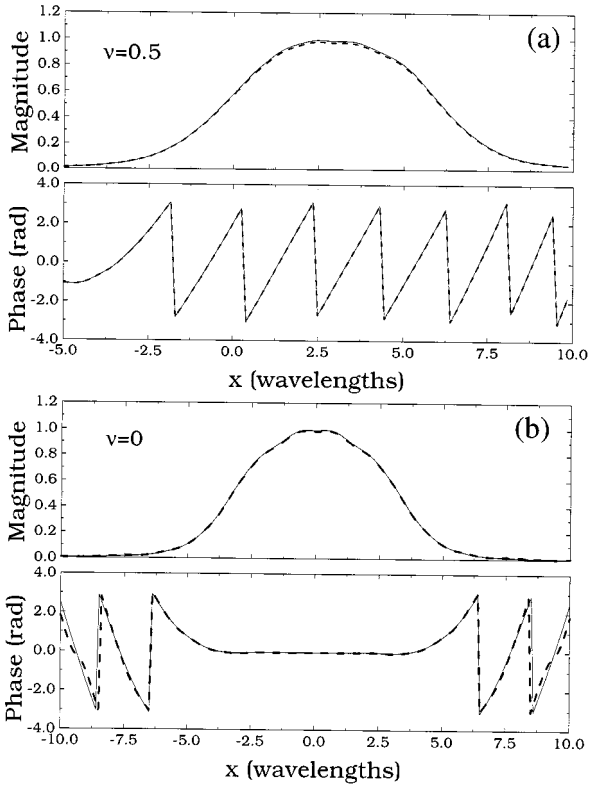

Fig. 4. Cosine-tapered aperture field in (20) ($d = 10\lambda_0$): Radiated near-zone field with $z_A = 10\lambda_0$, $z_{obs} = 5\lambda_0$. (a) $\nu = 0.5$, $L_x = 0.0125d = 0.125\lambda_0$ (i.e., 80 beams). (b) $\nu = 0$, $L_x = 0.1d = \lambda_0$ (i.e., ten beams). (—) Reference solution [Kirchhoff integration in (2)]. (- - -) Beam-computed from (13), with (15) and (19).

III. Reflection From and Transmissions Through a Smoothly Curved Dielectric Interface: Canonical Problem

A. Problem Strategy

Before considering the interaction of the beam-based incident field in Section II with the rough surface profile sketched in Fig. 1, we treat the canonical problem of interaction with a smoothly curved portion of that profile as shown in Figs. 5 and 6.

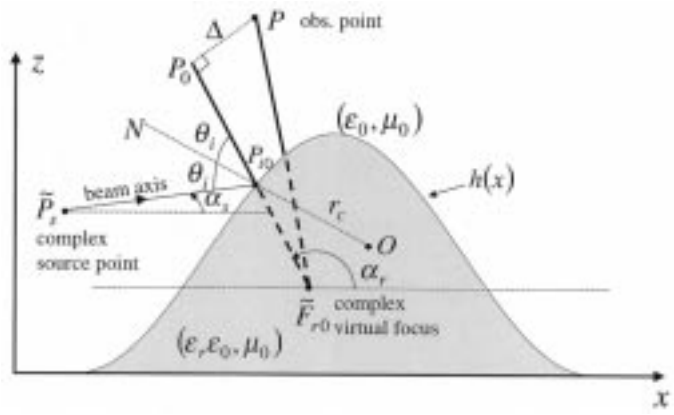

Fig. 5. Beam reflection from a curved dielectric interface. α_s = real departure angle of incident beam axis with respect to the x-axis; α_r = real departure angle of reflected beam axis with respect to the x-axis; and θ_i = real incidence/reflection angle with respect to the surface normal N at P_{i0}; r_c = surface radius of curvature at P_{i0}.

The beam-based synthesis of the reflected and transmitted fields can be constructed by propagating each of the incident narrow-waisted basis beams in Sections II-B and -C through the environment and recombining thereafter. Because the asymptotic basis beams are parameterized in terms of a source point in the complex coordinate space, they propagate in complex space along *complex* ray trajectories, which yield only a *single* physical point *at* the real space observer. This renders the field evaluation computation intensive. However, for narrow-waisted beams, one may utilize a paraxial approximation scheme, which leads to *almost real* ray tracing [3], [14] that is only slightly different from (and even computationally cheaper than) standard ray tracing from the Kirchhoff integration (2) in *real* configuration space.

B. Reflected Field

The problem geometry is illustrated in Fig. 5. An incident Gaussian beam is generated by a CSP at

$$\tilde{P}_s = (x_s + ib\cos\alpha_s,\, z_s + ib\sin\alpha_s) \tag{21}$$

with α_s being the *real* departure angle of the incident beam axis with respect to the x-axis. As shown in [14], for electrically large and smooth scatterers, and when the observation point $P = (x, z)$ lies in the paraxial region of the reflected beam [$\Delta \ll (|\overline{\tilde{F}_{r0}P_0}|^2 + b^2)^{1/2}$ in Fig. 5], the reflected field can be approximated in terms of the on-axis field (at P_0) and a complex phase correction. Denoting the on-axis parameters by the subscript zero, one finds for the y-directed electric field [14]

$$\begin{aligned} E^{refl}(P) &\approx E^{refl}(P_0)\big|_{\tilde{P}_i = P_{i0}} \exp\left(ik_0\tilde{\delta}_p\right) \\ &= \Gamma E^{\text{inc}}(P_{i0}) \left(\frac{\tilde{f}_{r0}}{\tilde{R}_0}\right)^{1/2} \exp\left[ik_0\left(L_{r0} + \tilde{\delta}_p\right)\right] \end{aligned} \tag{22}$$

where (see Fig. 5)

$$\tilde{R}_0 = \overline{\tilde{F}_{r0}P_0}, \qquad L_{r0} = \overline{P_{i0}P_0} \tag{23}$$

and $\tilde{\delta}_p$ is the complex phase correction

$$\tilde{\delta}_p = \tilde{R} - \tilde{R}_0, \qquad \tilde{R} = \overline{\tilde{F}_{r0}P}. \tag{24}$$

Moreover, $\tilde{F}_{r0} = (\tilde{x}_{fr0}, \tilde{z}_{fr0})$ is the *complex* virtual focus obtained via analytic continuation of the standard ray-optical formulas (see [21, p. 169]), but approximating the *complex* incidence point $\tilde{P}_i$ by the *real* beam-axis incidence point $P_{i0} = (x_{i0}, z_{i0})$

$$\tilde{x}_{fr0} = x_{i0} - \tilde{f}_{r0}\cos\alpha_r, \qquad \tilde{z}_{fr0} = z_{i0} - \tilde{f}_{r0}\sin\alpha_r \tag{25}$$

$$\tilde{f}_{r0} = \frac{\tilde{L}_{i0} r_c \cos\theta_i}{2\tilde{L}_{i0} + r_c\cos\theta_i}, \qquad \tilde{L}_{i0} = \overline{\tilde{P}_s P_{i0}}. \tag{26}$$

Here, α_r is the real departure angle of the reflected beam axis with respect to the x-axis, r_c is the curvature radius at P_{i0}

$$r_c = -\frac{\left[1 + (h'(x_{i0}))^2\right]^{3/2}}{h''(x_{i0})}, \qquad ' \equiv d/dx \tag{27}$$

and Γ is the TM plane-wave reflection coefficient

$$\Gamma = \frac{\cos\theta_i - \sqrt{\epsilon_r - \sin^2\theta_i}}{\cos\theta_i + \sqrt{\epsilon_r - \sin^2\theta_i}} \tag{28}$$

where ϵ_r is the dielectric relative permittivity and θ_i is the real incidence angle with respect to the surface normal N at P_{i0}.

As shown in [14], this corresponds to tracing a ray along a *complex* trajectory from the CSP at $\tilde{P}_s$ to the intersection of the *real* beam axis with the *real* surface; from there, the path to the observer proceeds entirely in *real* configuration space, along the beam axis. Also presented in [14] are further corrections, obtained by expanding the analytic continuation of the reflection coefficient Γ in (28) and of the divergence coefficient

$$\tilde{D}_r = \left[\frac{\left(\overline{\tilde{P}_s\tilde{P}_i} + \overline{\tilde{P}_i P}\right) r_c\cos\tilde{\theta}_i}{2\overline{\tilde{P}_s\tilde{P}_i}\,\overline{\tilde{P}_i P} + \left(\overline{\tilde{P}_s\tilde{P}_i} + \overline{\tilde{P}_i P}\right) r_c\cos\tilde{\theta}_i}\right]^{1/2}$$
$$\tilde{\theta}_i \equiv \theta_i|_{P_{i0}=\tilde{P}_i} \tag{29}$$

in Taylor series about their on-axis values. Actually, these corrections are more cumbersome to generate; we obtained acceptable results by using only the phase correction in (24). Multiple reflections can be incorporated by iterating (22) whereby [with proper definition of the square root in (17)] the complex focus determined at each iteration becomes the phase reference for the next iteration (see Appendix A). Again, apart from the complex ray connecting the CSP to the first real incidence point, the multihop path to the observer proceeds entirely in *real* configuration space along the beam axes, and the phase correction is applied only to the last beam segment that reaches the observer.

C. Transmitted Field

The same considerations applied to the transmitted field (see Fig. 6) yield [14]

$$E^{tr}(P) \approx E^{tr}(P_0)\big|_{\tilde{P}_i=P_{i0}} \exp(ik\tilde{\delta}_p)$$
$$= TE^{\text{inc}}(P_{i0})\left(\frac{\tilde{f}_{t0}}{\tilde{R}_0}\right)^{1/2} \exp\left[ik_0\left(L_{t0} + \sqrt{\epsilon_r}\tilde{\delta}_p\right)\right] \tag{30}$$

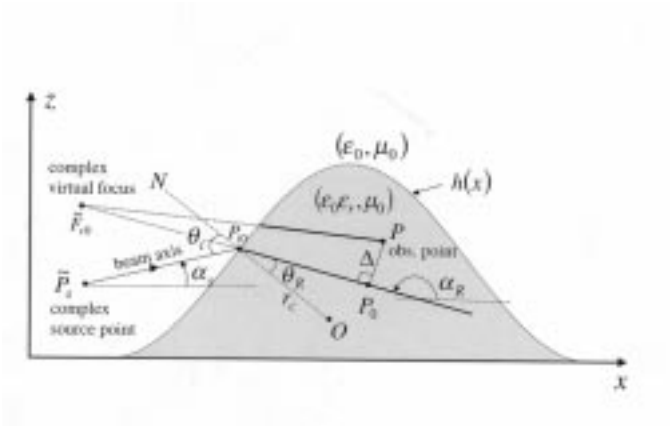

Fig. 6. Beam transmission through a curved dielectric interface. α_R and θ_R are the refracted (transmitted) real departure angles with respect to the x-axis and the surface normal N at P_{i0}, respectively.

where $k = k_0\sqrt{\epsilon_r}$ and

$$\tilde{R}_0 = \overline{\tilde{F}_{t0}P_0}, \qquad L_{t0} = \overline{P_{i0}P_0} \tag{31}$$

$$\tilde{\delta}_p = \tilde{R} - \tilde{R}_0, \qquad \tilde{R} = \overline{\tilde{F}_{t0}P} \tag{32}$$

$$\tilde{F}_{t0} = (x_{i0} + \tilde{f}_{t0}\cos\alpha_R, z_{i0} + \tilde{f}_{t0}\sin\alpha_R) \tag{33}$$

$$\tilde{f}_{t0} = \frac{\tilde{L}_{i0} r_c\cos\theta_R}{(\Omega-1)\tilde{L}_{i0} + \Omega r_c\cos\theta_i}, \qquad \Omega = \frac{\cos\theta_i}{\sqrt{\epsilon_r}\cos\theta_R} \tag{34}$$

$$T = 1 + \Gamma \tag{35}$$

with α_R denoting the real departure angle of the transmitted beam axis with respect to the x-axis and θ_R denoting the refraction angle, with respect to the surface normal N at P_{i0}, according to Snell's law

$$\sin\theta_i = \sqrt{\epsilon_r}\,\sin\theta_R. \tag{36}$$

As before, this approximation corresponds to tracing a complex ray from the CSP to the real incidence point and then a real ray to the observer [14]. Note that in the presence of a slightly lossy dielectric as in Fig. 8, the refraction angle θ_R becomes complex. In that case, we still use a real refracted ray, propagating along the direction $\mathrm{Re}(\theta_R)$. Multiple reflections/transmissions can be handled by iterating and combining (22) and (30), following the guidelines given in Section III-B.

IV. Reflection From and Transmission Through a Moderately Rough Dielectric Interface

We now address the "real problem" geometry in Fig. 1, using the building blocks of Sections II-B, II-C, and III.

A. The Multiply Reflected/Transmitted Beam Algorithm

The main steps of the proposed algorithm can be summarized as follows.

1) *Aperture Field Discretization.* The narrow-waisted CSP algorithm (15)–(19) in Sections II-B and -C is applied to the given aperture field distribution and yields the Gabor-weighted beam amplitudes.
2) *Beam-Axes Tracing.* The beam axes follow real-ray trajectories in real configuration space. For each beam

launched at the aperture plane, the axis trajectories after intersection at an interface are governed by Snell's laws of reflection and transmission (see Figs. 5 and 6). The hierarchy of possible multiple (reflection/transmission) bifurcations at each encounter with the *rough* interface can be organized formally through use of a binary-tree data structure [22], whose *nodes* contain the relevant data (i.e., incidence point, departure angle, etc.). However, in our applications here, we shall rely primarily on the first, and possibly also the second, bifurcation.

3) *Beam Parameter Computation.* Having determined the beam axis topology, the other relevant parameters for each beam segment (e.g., reflection/transmission coefficients, complex foci, phase lag) are computed recursively, starting from the initial complex source point and progressively scanning the binary tree (see Appendix A).
4) *Beam Field Computation.* Each reflected/transmitted Gabor-weighted beam field contribution at the observer is computed via the quasiray paraxial approximations (22)–(28) and (30)–(36) described in Section III. As already stated, in the presence of multiple interactions, the complex phase correction is applied only to the last beam segment that reaches the observer (see Appendix A).
5) *Beam Summation for Total Field.* The individual reflected/transmitted beam contributions are recombined to yield the total field at the observer.

In principle, the above multiple interaction algorithm is able to account for possible evanescent contributions (total reflection). We have not explored this aspect so far and have, in fact, restricted the problem conditions in the numerical tests of Section IV-B so that total reflection does not occur. Also excluded are near-grazing incidence contributions, which require more sophisticated propagation models than those in Section III. Note also that in [2], [3], the narrow-waisted beam algorithm is applied to propagation through planar and circular cylindrical dielectric layers where the beam tracing can be performed analytically; in our problem, due to the irregular form of the interface profile $h(x)$ (see Fig. 1), a numerical procedure is required.

B. Example Problems and Numerical Results

In the problem geometry of Fig. 1, the TM-polarized field generated by the nonphased cosine-tapered aperture field distribution in (20) (with $\nu = 0$) is assumed to impinge from free space onto a moderately rough interface described by the continuous function $h(x)$, which in the examples below is parameterized by a quartic-spline [23]

$$h(x) = \sum_{n=-4}^{N_h-1} c_n s_4(x - x_n), \qquad x_{\min} \le x \le x_{\max} \tag{37}$$

$$x_n = x_{\min} + n\Delta_x, \qquad \Delta_x = (x_{\max} - x_{\min})/N_h \tag{38}$$

with $s_4(\cdot)$ representing the standard quartic B-spline basis function (Fig. 7) [23]. Because of this parameterization, most of the beam tracing computational tasks (solution of fourth-degree algebraic equations) can be performed *analytically*. The aperture width is adjusted so as to illuminate most of the region of interest, with edge effects deemphasized due to the aperture profile tapering. Since we intend to apply the beam method to detection and identification of buried objects, the dielectric half-space parameters have been chosen to simulate soil conditions [24]. The reflected and transmitted fields for this configuration have been computed via the beam algorithm detailed in Sections II and III and compared with a reference solution obtained by the Leviatan–Boag multifilament current method [25]. Although this method was introduced in [25] for cylindrical scatterers, its application to the rough surface geometry is justified in Appendix B. Since beam superposition is a high-frequency (HF) method, the rough surface parameters were adjusted so as to guarantee a minimum curvature radius of about 4.2 free-space wavelengths and a maximum slope of about 34° (see Fig. 8). This places the wave dynamics well within the range for HF asymptotic localization. Note that the dielectric is slightly lossy so that the remarks in Section III-C apply. It should be mentioned that we have previously applied the algorithm to reflection from a perfectly conducting sinusoidal profile and have calibrated its range of validity there [26]. The results from this test case have guided our choice of problem parameters here.

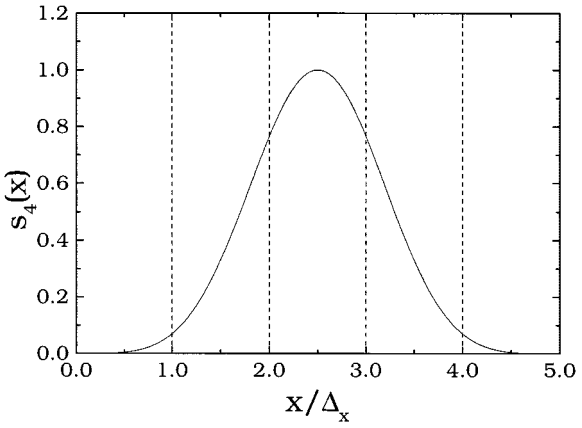

Fig. 7. Quartic B-spline basis function $s_4(x)$.

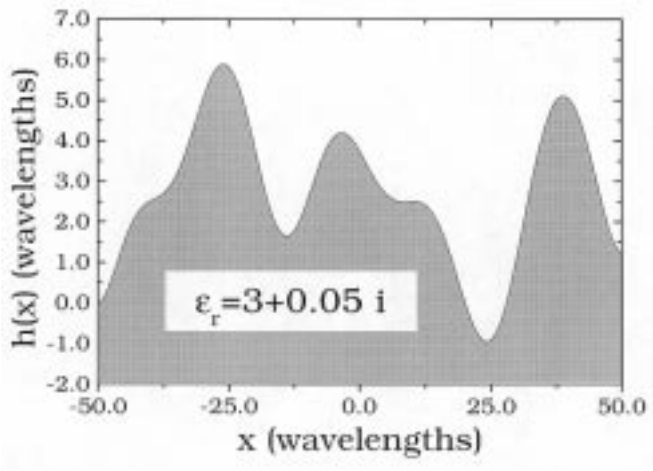

Fig. 8. Rough surface geometry and parameters. Relative permittivity: $\epsilon_r = 3 + i0.05$; maximum slope: 34°; minimum curvature radius: $4.2\lambda_0$; maximum height: $5.88\lambda_0$. The chosen permittivity models a class of realistic soil conditions.

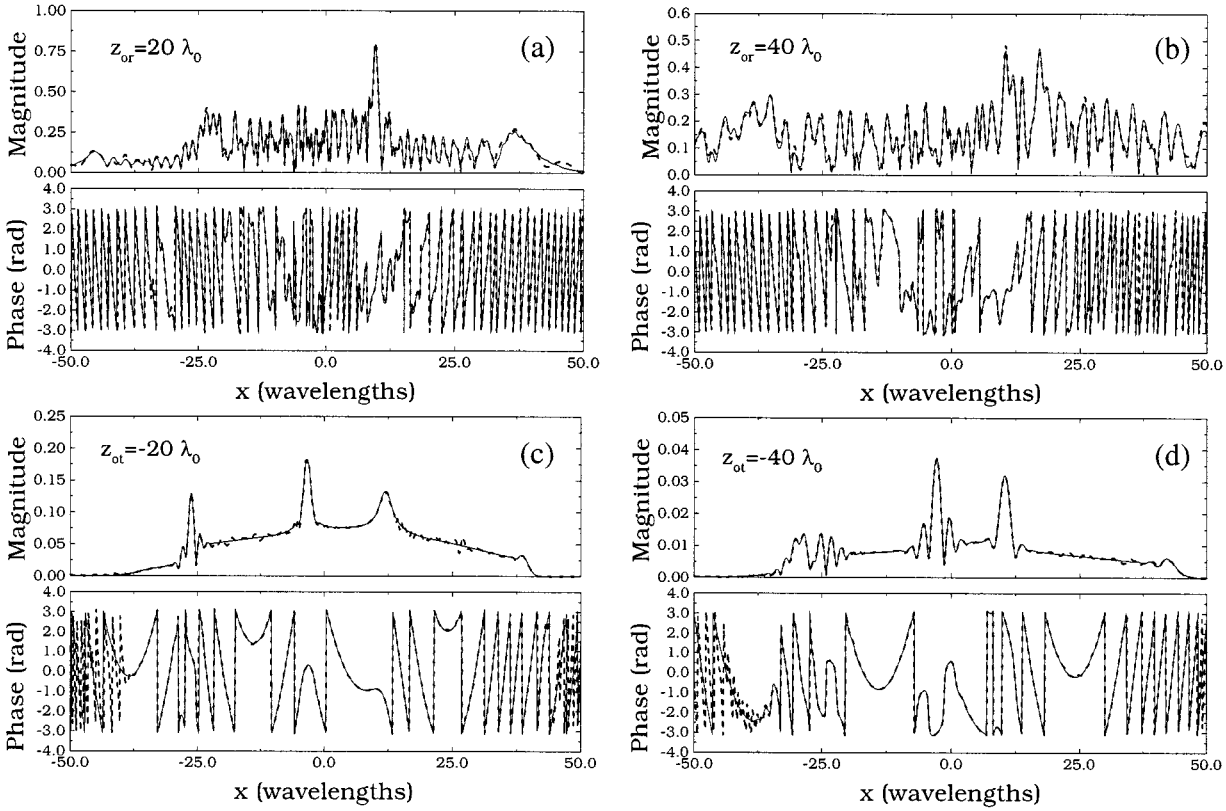

Fig. 9. Beam-computed reflected/transmitted fields and Leviatan–Boag reference solution in various observation planes. Parameters as in Fig. 8. Aperture width: $d = 80\lambda_0$; aperture height: $z_A = 6.4\lambda_0$ (i.e., $0.52\lambda_0$ above maximum profile height); beam lattice period: $L_x = 0.0125d = \lambda_0$ (i.e., 80 beams). (a) Reflected field at $z_{0r} = 20\lambda_0$. (b) Reflected field at $z_{0r} = 40\lambda_0$. (c) Transmitted field at $z_{0t} = -20\lambda_0$. (d) Transmitted field at $z_{0t} = -40\lambda_0$. (—) Reference solution and (- - -) beams.

In Fig. 9, for a fixed beam-lattice configuration and the problem parameters in Fig. 8, the beam-computed reflected and transmitted fields at various observation planes are compared with the reference solution. Here, the aperture is located $0.52\lambda_0$ away from the nearest portion of the interface profile, thereby ensuring that the *individual* narrow-waisted paraxial GBs are collimated sufficiently to have them interact *locally* with the irregular surface. We found that in order to obtain robust and accurate predictions, the aperture distance to the profile should be no larger than a wavelength. As in [26], good agreement is verified for the beam/lattice parameters listed in the figure captions. The accuracy of the scattered/transmitted field synthesis improves for *greater observation distance* because of the *collective* behavior of the beams in the far-zone paraxial approximation. The agreement is satisfactory even at moderate observation distances, despite some slight local deviations. As in [1]–[3], numerical insensitivity to beam/lattice parameter scramblings is taken as a pragmatic performance criterion for robustness of the algorithm (see Fig. 10). This feature permits *a priori* accuracy assessments when reference solutions are not available; note that the pragmatic scrambling criterion used here aims at an *adequate* number of beams, without any attempt to minimize that number. For the nonphased aperture example, we found the best tradeoff between accuracy and computational cost for $L_x \sim \lambda_0$. A finer sampling may, however, be required for phased aperture field distributions. It should be emphasized that the accuracy deteriorates with increasing distance of the aperture from the nearest point on the surface profile. As noted

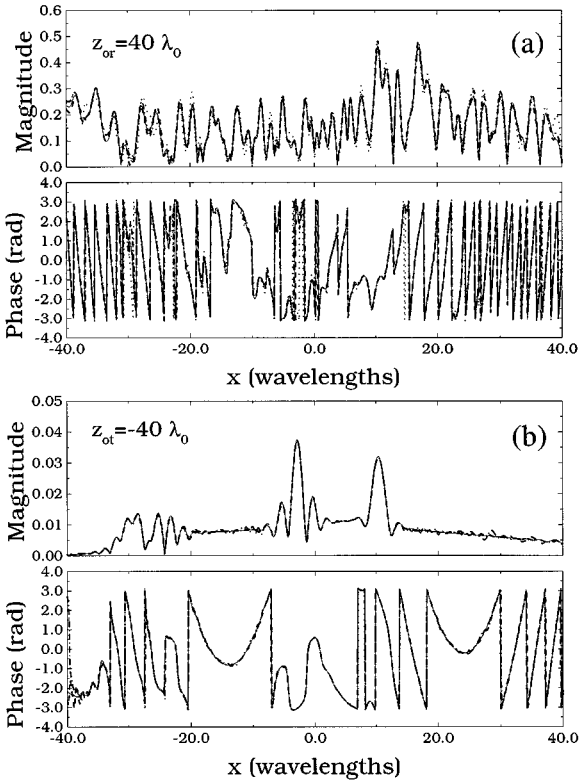

Fig. 10. (a) As in Fig. 9(b), but with various beam lattice periods. (b) As in Fig. 9(d), but with various beam lattice periods. (—) Reference solution; (· · · · · ·) 134 beams ($L_x = 0.0075d$); (- - -) 80 beams ($L_x = 0.0125d$); and (-·-·-·-) 58 beams ($L_x = 0.0175d$).

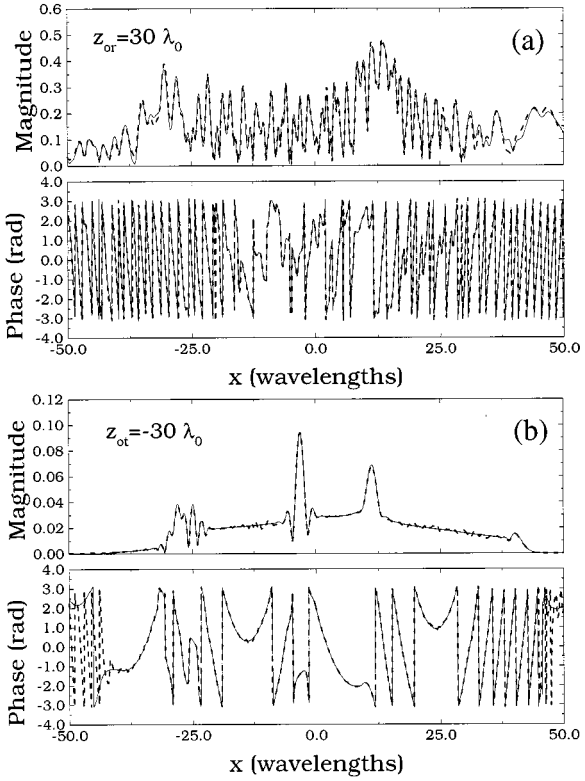

Fig. 11. As in Fig. 9, but with aperture plane at $z_A = 35.9\lambda_0$. Multistep beam algorithm: i) Narrow-waisted beam discretization at $z = z_A$ with $L_x = 0.01d$ (i.e., 100 beams). ii) Beam-computed incident field projection onto a *virtual* aperture at $z_V = 6.4\lambda_0$ as in Fig. 9, to restore the local sampling capability of the surface profile by the individual basis beams. iii) Narrow-waisted beam decomposition at $z = z_V$ with $L_x = 0.0125d = \lambda_0$ (i.e., 80 beams) as in Fig. 9. iv) Beam-tracing paraxial-approximation scheme. (a) Reflected field at $z_{or} = 30\lambda_0$. (b) Transmitted field at $z_{ot} = -30\lambda_0$. The maximum height of the profile in Fig. 8 is $5.88\lambda_0$. (—) Reference solution and (- - -) beams.

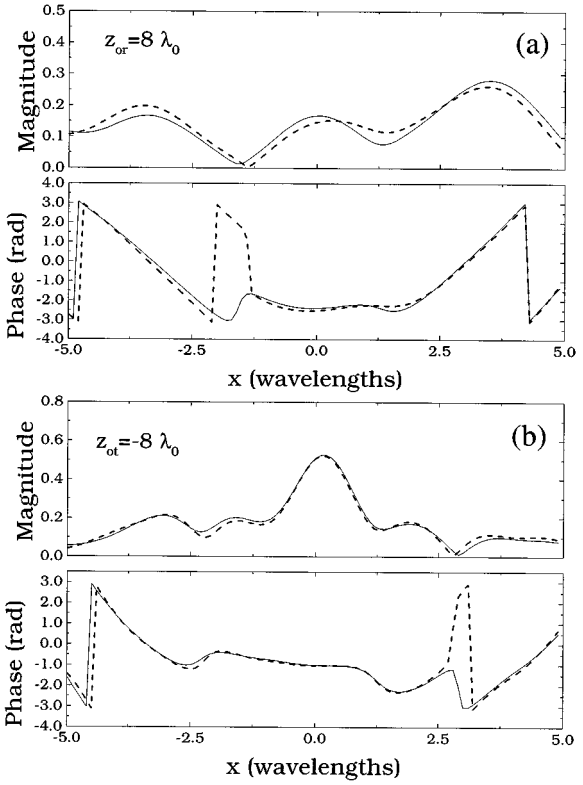

Fig. 12. Rough interface profile as in Fig. 8, but scaled so as to have maximum slope: 34°; minimum curvature radius: $0.42\lambda_0$; maximum height: $0.588\lambda_0$. Beam-computed reflected/transmitted fields and Leviatan–Boag reference solutions. Aperture width: $d = 8\lambda_0$; aperture height: $z_A = 0.8\lambda_0$; beam lattice period: $L_x = 0.1d = 0.8\lambda_0$ (i.e., ten beams). (a) Reflected field at $z_{0r} = 8\lambda_0$. (b) Transmitted field at $z_{0t} = -8\lambda_0$. (—) Reference solution and (- - -) beams.

above, to *establish* the scattered/transmitted field by local beam sampling of the interface profile, the aperture must be close enough to the surface so that the rapid spread of the beams at greater distances has not yet taken place. However, this is not a severe limitation, since, as shown in Fig. 11, it is possible to perform a two-step Gabor decomposition, i.e., projecting the beam-computed radiated field onto a virtual aperture (within a wavelength above the surface so as to restore the local sampling capability) and then again applying the (narrow-waisted) beam algorithm. The additional cost is computationally minimal because of the highly efficient evaluation of the Gabor coefficients for narrow-waisted beams [see (19)]. Even for relatively "low-frequency" geometries with critical dimensions on the order of a wavelength or less, the beam algorithm, though no longer *highly* accurate, may still be able to provide reasonably good predictions. For *small* radius of curvature portions on the roughness profile, this is demonstrated in Fig. 12, with the problem parameters given in the figure caption. Of course, each such excursion into the "low-frequency" range must be validated independently by the scrambling criterion, but it is worth noting that such attempts need not to be doomed to failure *a priori*. Although the beam algorithm performance assessments here are based on the single example depicted in Figs. 7 and 8, we emphasize that confidence in these assessments has been established by an extensive sequence of relevant prior numerical calibration experiments. In particular, we have found accurate results for moderate roughness with maximum slopes $\lesssim 40°$ and (average) curvature radii larger than a wavelength, and for indidence directions far from grazing [$\nu \lesssim \sin 30°$ in (20)]. We have also performed simulations for very high and low dielectric contrasts with $\mathrm{Re}(\epsilon_r)$ ranging from 1.2 to 10 and $\mathrm{Im}(\epsilon_r)$ up to 0.5; the quality of results was found to be similar to those for the case of Fig. 8. Concerning computing times, for the most expensive (two-step) implementation described in Fig. 11, we found about 9 ms to compute the field at a single position on a 500-MHz laptop; no particular effort was made to optimize the numerical code.

V. Concluding Remarks

A previously developed, rigorous, self-consistent, quasi-ray, narrow-waisted beam algorithm [1]–[3] has been reexamined and applied to the new problem of EM transmission and reflection in the presence of moderately rough surfaces.

The narrow-waisted beams are wave objects with very short collimation lengths and therefore act like *almost real* ray fields. The rigorous complex ray machinery that is required for arbitrary complex source point beams can thus be reduced to *almost real* ray asymptotics, which, however, avoids failures near caustics and other ray-field transition regions. Due to its rapid spreading, the paraxial approximations described in Section III are of little use for tracking a *single* narrow-waisted beam away

from an aperture into the far zone. However, as observed in [2] and [3], when treated *collectively* as an *ensemble*, each paraxial beam can be tracked locally to and from dielectric interfaces with large radius of curvature. Apart from the paraxial beam-tracing procedure, the computational complexity of the beam algorithm is $\mathcal{O}(N_b)$, with N_b being the number of beams in the expansion. In contrast to standard ray methods, time-consuming eigenray search for evaluating the field at a given observation point is avoided, and the beam tracing needs to be performed *only once* (phrased in another way, we are interested in reliably evaluating the actual field at the observer without worrying about which appropriately weighted individual beam contributions establish that field). The algorithm has been calibrated against a reference (full-wave) solution, and will be exploited as a fast forward solver in the interface profile estimation problem [4]. A two-step beam decomposition may be required when the aperture is "sufficiently far" from the scatterer. In this case, the computational complexity is of the same order as the physical optics (PO) Kirchhoff approximation for a dielectric interface. However, the beam algorithm usually allows a coarser discretization, so that N_b is typically smaller than the corresponding number of PO integration points in the Kirchhoff integral [see (2), but applied to integration along the interface profile] for specified accuracy. In addition, the beam algorithm is potentially able to accommodate multiple interactions in a simpler fashion. The algorithm can be extended to pulsed excitations [27].

APPENDIX A
MULTIPLE REFLECTIONS

Consider an incident Gaussian beam generated by the CSP in (21). Denoting by $P_{i0}^{(j)} = (x_{i0}^{(j)}, z_{i0}^{(j)})$, $j = 1, \ldots, N_r$, the real incidence points from which emerge the (real ray) reflected beam axes, and by $P_{i0}^{(N_r+1)} = P_0$ the orthogonal projection of the observation point P onto the axis of the (N_r+1)th beam that reaches the observer, the far-zone paraxial approximation (22) can be generalized as follows (implementing the procedure outlined at the end of Section III-B):

$$E^{refl}(P) \approx E^{\mathrm{inc}}(P_{i0}^{(1)}) \exp\left(ik_0 \tilde{\delta}_p^{(N_r)}\right) \cdot \prod_{j=1}^{N_r} \Gamma^{(j)} \left(\frac{\tilde{f}_{r0}^{(j)}}{\tilde{R}_0^{(j)}}\right)^{1/2} \exp\left(ik_0 L_{r0}^{(j)}\right) \tag{39}$$

where

$$\tilde{R}_0^{(j)} = \overline{\tilde{F}_{r0}^{(j)} P_{i0}^{(j+1)}}, \qquad L_{r0}^{(j)} = \overline{P_{i0}^{(j)} P_{i0}^{(j+1)}} \tag{40}$$

$$\tilde{F}_{r0}^{(j)} = \left(x_{i0}^{(j)} - \tilde{f}_{r0}^{(j)} \cos\alpha_r^{(j)},\ z_{i0}^{(j)} - \tilde{f}_{r0}^{(j)} \sin\alpha_r^{(j)}\right) \tag{41}$$

$$\tilde{f}_{r0}^{(j)} = \frac{\tilde{L}_{i0}^{(j)} r_c^{(j)} \cos\theta_i^{(j)}}{2\tilde{L}_{i0}^{(j)} + r_c^{(j)} \cos\theta_i^{(j)}} \tag{42}$$

$$\tilde{L}_{i0}^{(1)} = \overline{\tilde{P}_s P_{i0}^{(1)}}, \qquad \tilde{L}_{i0}^{(j)} = \overline{\tilde{F}_{r0}^{(j-1)} P_{i0}^{(j)}}, \qquad j \geq 2 \tag{43}$$

$$r_c^{(j)} = -\frac{\left[1 + (h'(x_{i0}^{(j)}))^2\right]^{3/2}}{h''(x_{i0}^{(j)})} \tag{44}$$

$$\Gamma^{(j)} = \frac{\cos\theta_i^{(j)} - \sqrt{\epsilon_r \sin^2 - \theta_R^{(j)}}}{\cos\theta_i^{(j)} + \sqrt{\epsilon_r - \sin^2\theta_R^{(j)}}} \tag{45}$$

$$\tilde{\delta}_p^{(N_r)} = \tilde{R}^{(N_r)} - \tilde{R}_0^{(N_r)}, \qquad \tilde{R}^{(N_r)} = \overline{\tilde{F}_{r0}^{(N_r)} P}. \tag{46}$$

In the above expressions, $\theta_i^{(j)}$ and $\alpha_r^{(j)}$ represent the real incidence angle [with respect to the surface normal at $P_{i0}^{(j)}$] and the real reflected beam axis departure angle (with respect to the x-axis) at the jth reflection, respectively.

APPENDIX B
REFERENCE SOLUTION

The multifilament–current method in [25] has been applied originally to scattering by, and transmission through, dielectric cylinders, but it can be easily adapted to smoothly irregular scatterers or moderately rough interfaces. The extension is based on the expansion of the internal and external unknown fields in terms of basis functions generated by suitably placed line sources. As in many numerical techniques, the unknown expansion coefficients are determined by solving a linear system obtained by enforcing the continuity boundary conditions of the tangential fields at selected points on the dielectric interface. In the resulting algorithm, the obtained numerical solution satisfies Maxwell's equations by construction, and its convergence and consistency are controlled by monitoring the error (discontinuity) in the boundary conditions at the dielectric interface between the matching points [25]. In our simulations, we chose the relevant parameters so as to ensure a 0.01% maximum error in the boundary conditions.

ACKNOWLEDGMENT

The authors gratefully acknowledge helpful comments by the anonymous referees.

REFERENCES

[1] J. J. Maciel and L. B. Felsen, "Systematic study of fields due to extended apertures by Gaussian beam discretization," *IEEE Trans. Antennas Propagat.*, vol. 37, pp. 884–892, July 1989.

[2] ——, "Gaussian beam analysis of propagation from an extended aperture distribution through dielectric layers, Part I—Plane layer," *IEEE Trans. Antennas Propagat.*, vol. 38, pp. 1607–1617, Oct. 1990.

[3] ——, "Gaussian beam analysis of propagation from an extended aperture distribution through dielectric layers, Part II—Circular cylindrical layer," *IEEE Trans. Antennas Propagat.*, vol. 38, pp. 1618–1624, Oct. 1990.

[4] V. Galdi, D. A. Castañon, and L. B. Felsen, "Multifrequency reconstruction of moderately rough interfaces via quasi-ray Gaussian beams," IEEE Trans. Geosci. Remote Sensing, submitted for publication.

[5] A. Ishimaru, *Wave Propagation and Scattering in Random Media*. New York: Academic, 1978.

[6] F. G. Bass and I. M. Fucks, *Wave Scattering from Statistically Rough Surfaces*. New York: Pergamon, 1979.

[7] P. Beckman and A. Spizzichino, *Scattering of Electromagnetic Waves from Rough Surfaces*. New York: Artech House, 1987.

[8] E. I. Thorsos, "The validity of the Kirchhoff approximation for rough surface scattering using a Gaussian roughness spectrum," *J. Acoust. Soc. Amer.*, vol. 83, pp. 78–82, Aug. 1988.

[9] F. D. Hastings, J. B. Schneider, and S. L. Broschat, "A Monte-Carlo FDTD technique for rough surface scattering," *IEEE Trans. Antennas Propagat.*, vol. 43, pp. 1183–1191, Nov. 1995.

[10] K. Sarabandi, Y. Oh, and F. T. Ulaby, "Numerical simulation of scattering from one-dimensional inhomogeneous dielectric random surfaces," *IEEE Trans. Geosci. Remote Sensing*, vol. 34, pp. 425–432, Mar. 1996.
[11] A. Collaro, G. Franceschetti, M. Migliaccio, and D. Riccio, "Gaussian rough surfaces and Kirchhoff approximation," *IEEE Trans. Antennas Propagat.*, vol. 47, pp. 392–398, Feb. 1999.
[12] Q. Li, C. H. Chan, and L. Tsang, "Monte Carlo simulations of wave scattering from lossy dielectric random rough surfaces using the physics-based two-grid method and the canonical-grid method," *IEEE Trans. Antennas Propagat.*, vol. 47, pp. 752–763, Apr. 1999.
[13] T. Dogaru and L. Carin, "Multiresolution time domain analysis of scattering from a rough dielectric surface," *Radio Sci.*, vol. 35, no. 6, pp. 1279–1292, Nov./Dec. 2000.
[14] Y. Z. Ruan and L. B. Felsen, "Reflection and transmission of beams at a curved interface," *J. Opt. Soc. Amer. A*, vol. 3, no. 4, pp. 566–579, Apr. 1986.
[15] B. Z. Steinberg, H. Heyman, and L. B. Felsen, "Phase-space beam summation for time-harmonic radiation from large apertures," *J. Opt. Soc. Amer. A*, vol. 8, pp. 41–59, Jan. 1991.
[16] M. J. Bastiaans, "Gabor's expansion of a signal into Gaussian elementary signals," *Proc. IEEE*, vol. 68, pp. 538–539, 1980.
[17] ——, "A sampling theorem for the complex spectrogram, and Gabor's expansion of a signal in Gaussian elementary signals," *Opt. Eng.*, vol. 20, pp. 594–598, 1981.
[18] P. D. Einziger and M. Shapira, "Gabor representation and aperture theory," *J. Opt. Soc. Amer. A*, vol. 3, no. 4, pp. 508–522, Apr. 1986.
[19] B. Z. Steinberg, H. Heyman, and L. B. Felsen, "Phase-space methods for radiation from large apertures," *Radio Sci.*, vol. 26, no. 1, pp. 219–227, Jan./Feb. 1991.
[20] V. Galdi, L. B. Felsen, and D. A. Castañon, "Narrow-waisted Gaussian beam discretization for short-pulse radiation from one-dimensional large apertures," *IEEE Trans. Antennas Propagat.*, vol. 49, pp. 1322–1332, Sept. 2000.
[21] L. B. Felsen and N. Marcuvitz, *Radiation and Scattering of Waves*. Piscataway, NJ: IEEE Press, 1994.
[22] J. L. Gross and J. Yelley, *Graph Theory and its Applications*. Boca Raton, FL: CRC Press, 1998.
[23] L. L. Shumaker, *Spline Functions: Basic Theory*. New York: Wiley, 1981.
[24] J. E. Hipp, "Soil electromagnetic parameters as functions of frequency, soil density, and soil moisture," *Proc. IEEE*, vol. 62, pp. 98–103, Jan. 1974.
[25] Y. Leviatan and A. Boag, "Analysis of electromagnetic scattering from dielectric cylinders using a multifilament current model," *IEEE Trans. Antennas Propagat.*, vol. AP-35, pp. 1119–1127, Oct. 1987.
[26] L. B. Felsen and V. Galdi, "Complex-source-point narrow-waisted ray-like Gaussian beams for frequency and time domain radiation and scattering," in *Ultra-Wideband, Short Pulse Electromagnetics 5*, S. R. Cloude and P. D. Smith, Eds. New York: Kluwer/Plenum, 2001.
[27] V. Galdi, L. B. Felsen, and D. A. Castañon, "Quasi-ray Gaussian beam algorithm for short-pulse two-dimensional scattering by moderately rough interfaces," IEEE Trans. Antennas Propagat., vol. 49, submitted for publication.

Vincenzo Galdi (M'98) was born in Salerno, Italy, on July 28, 1970. He received the Laurea degree *(summa cum laude)* in electrical engineering and the Ph.D. degree in applied electromagnetics from the University of Salerno, Italy, in 1995 and 1999, respectively.

From April to December 1997, he held a Visiting Position in the Radio Frequency Division of the European Space Research & Technology Centre (ESTEC-ESA), Noordwijk, The Netherlands, where he was involved in developing CAD tools for microwave filters and phased-array antennas with coaxial excitation. In September 1999, he received a European Union postdoctoral fellowship through the University of Sannio, Benevento, Italy. In October 1999, he became a Research Associate in the Department of Electrical and Computer Engineering, Boston University, Boston, MA, where he is currently working on wave-oriented imaging algorithms for landmine detection and classification. His research interests include analytical and numerical techniques for wave propagation in complex environments, path integrals, and stochastic resonance.

Dr. Galdi is the recipient of the 2001 International Union of Radio Science (URSI) "Young Scientist Award." He is a member of Sigma Xi.

Leopold B. Felsen (S'47–M'54–SM'55–F'62–LF'90) was born in Munich, Germany, on May 7, 1924. He received the B.E.E., M.E.E, and D.E.E. degrees from the Polytechnic Institute of Brooklyn, Brooklyn, NY, in 1948, 1950, and, 1952, respectively.

He emigrated to the United States in 1939 and served in the U.S. Army from 1943 to 1946. After 1952, he remained with the Polytechnic Institute of Brooklyn (now Polytechnic University), becoming a Professor in 1962 and University Professor in 1978. From 1974 to 1978, he was Dean of Engineering. In 1994, he resigned from the full-time Polytechnic Faculty and became University Professor Emeritus. He is now a part-time Professor of Aerospace and Mechanical Engineering and Professor of Electrical and Computer Engineering at Boston University, Boston, MA. He is the author or coauthor of more than 300 papers and several books, including *Radiation and Scattering of Waves* (Englewood Cliffs, NJ: Prentice-Hall, 1973; Piscataway, NJ: IEEE Press, 1994). He is an Associate Editor of several professional journals and an editor of the *Wave Phenomena Series* (New York: Springer-Verlag). His research interests encompass wave propagation and diffraction in complex environments and in various disciplines, high-frequency asymptotic and short-pulse techniques, and phase-space methods with an emphasis on wave-oriented data processing and imaging.

Dr. Felsen is a member of Sigma Xi and a Fellow of the Optical Society of America and the Acoustical Society of America. He has held named Visiting Professorships and Fellowships at universities in the United States and abroad, including the Guggenheim in 1973 and the Humboldt Foundation Senior Scientist Award in 1981. In 1974, he was an IEEE Antennas and Propagation Society (APS) Distinguished Lecturer. He received the Balthasar van der Pol Gold Medal from the International Union of Radio Science (URSI) in 1975, an honorary doctorate from the Technical University of Denmark in 1979, the IEEE Heinrich Hertz Gold Medal for 1991, the APS Distinguished Achievement Award for 1998, the IEEE Third Millennium Medal in 2000 (nomination by APS), three Distinguished Faculty Alumnus Awards from Polytechnic University, and an IEEE Centennial Medal in 1984. He also has received Best Paper awards for several papers in which he was an author or coauthor. In 1977, he was elected to the National Academy of Engineering. He served on the APS Administrative Committee from 1963 to 1966 and as Vice Chairman and Chairman for both the United States (1966–1973) and the International (1978–1984) URSI Commission B.

David A. Castañon (S'68–M'79–SM'98) received the B.S. degree in electrical engineering from Tulane University, New Orleans, LA, in 1971 and the Ph.D. degree in applied mathematics from the Massachusetts Institute of Technology (MIT), Cambridge, in 1976.

From 1976 to 1981, he was a Research Associate with the Laboratory for Information and Decision Systems, MIT. From 1982 to 1990, he was Senior and Chief Research Scientist at Alphatech, Inc., Burlington, MA. Since 1990, he has been a Professor in the Department of Electrical and Computer Engineering, Boston University, Boston, MA. His research interests include stochastic control and estimation, optimization, and image processing.

Dr. Castañon served as a member of the Board of Governors of the IEEE Control Systems Society. He is also a member of AMS, SIAM, and INFORMS.